Title
Magnetization and stability study of a cobalt-ferrite-based ferrofluid

Authors
Kamali, Saeed
Pouryazdan, Mohsen
Ghafari, Mohammad
et al.

Publication Date
2016-04-01

DOI
10.1016/j.jmmm.2015.12.007

Peer reviewed

Journal of Magnetism and Magnetic Materials 404 (2016) 143–147

Contents lists available at ScienceDirect

Journal of Magnetism and Magnetic Materials

journal homepage: www.elsevier.com/locate/jmmm

Magnetization and stability study of a cobalt-ferrite-based ferrofluid

Saeed Kamali [a,*], Mohsen Pouryazdan [b,c], Mohammad Ghafari [b,d], Masayoshi Itou [e], Masoud Rahman [f], Pieter Stroeve [f], Horst Hahn [b,c,d], Yoshiharu Sakurai [e]

[a] Department of Mechanical, Aerospace and Biomedical Engineering, University of Tennessee Space Institute, Tullahoma, TN 37388, USA
[b] Institute for Nanotechnology, Karlsruhe Institute of Technology, Karlsruhe, Germany
[c] Joint Research Laboratory Nanomaterials (KIT and TUD) at Technische Universität Darmstadt (TUD), 64287 Darmstadt, Germany
[d] Herbert Gleiter Institute of Nanoscience, Nanjing University of Science and Technology, Nanjing 210094, People's Republic of China
[e] Japan Synchrotron Radiation Research Institute, SPring-8, 1-1-1 Kouto, Sayo-cho, Sayo-gun, Hyogo 679-5198 Japan
[f] Department of Chemical Engineering and Materials Science, University of California, Davis, CA 95616, USA

ARTICLE INFO

Article history:
Received 3 September 2015
Received in revised form
9 November 2015
Accepted 1 December 2015
Available online 8 December 2015

Keywords:
Ferrofluid
Cobalt-ferrite
Nanoparticles
Mössbauer spectroscopy
Magnetic Compton scattering
Nano-magnetism

ABSTRACT

In this study the structural and magnetization properties of a $CoFe_2O_4$-based ferrofluid was investigated using x-ray diffraction (XRD), transmission electron microscopy (TEM), energy dispersive x-ray spectroscopy (EDS), Mössbauer spectroscopy, and magnetic Compton scattering (MCS) measurements. The XRD diagram indicates that the nanoparticles in the ferrofluid are inverse spinel and TEM graph shows that the ferrofluid consists of spherical nanoparticles with an average diameter of 18 ± 1 nm, in good agreement with the size, 19.4 nm, extracted from line broadening of the XRD peaks. According to EDS measurements the composition of the nanoparticles is $CoFe_2O_4$. Mössbauer spectroscopy shows that the cation distributions are $(Co_{0.38}Fe_{0.62})[Co_{0.62}Fe_{1.38}]O_4$. The MCS measurement, performed at 10 K, indicates that the magnetization of the nanoparticles is similar to magnetization of maghemite and magnetite. While the magnetization of the inverse spinels are in [111] direction, interestingly, the magnetization deduced from MCS is in [100] direction. The $CoFe_2O_4$-based ferrofluid is found to be stable at ambient conditions, which is important for applications.

1. Introduction

Ferrofluids, which are defined as stable colloidal magnetic nano-sized particles dispersed in a carrier liquid, have many industrial applications [1,2]. It is already well-known that the application of magnetic nanoparticles in general and iron-oxide and ferrite nanoparticles in particular is very wide due to their novel properties. They have various applications in different fields, ranging from new functional materials [3] such as magnetic recording media [4] to biomedical diagnostics and therapy [5] such as cancer treatment by hyperthermia [6]. Sufficiently small nanoparticles are magnetic single domain with a magnetic anisotropy energy of the same order as the thermal energy [7], and the atomic magnetic moments in these nanoparticles fluctuate between the easy axes directions giving rise to superparamagnetism [8–10]. Suspension of such nanoparticles in liquids, resulting in ferrofluids, makes them even more interesting and opens new routes of applications. This class of material was initially developed by NASA to be used in space to control fluids [11]. Besides their primary application as rotating shaft seals in satellites, they have found a lot of applications from being used in mechanical machines due to their interesting mechanical properties [12] to computer hard drives [1,2]. Ferrofluids have also many applications in medicine such as for sustaining drug attached to the surface of magnetic nanoparticles, at specific sites in the body by using external field [13] and for implantable artificial hearing aids in the form of ferrofluidic actuators [1]. It is worth mentioning that the magnetism in ferrofluids is more complicated compared to nano-powders owing to the existence of additional parameters such as existence of the Brownian motion, which is simultaneously a mechanism for rotation of magnetization direction in nanoparticles due to the particle rotation. Other parameters, such as interaction between magnetic nanoparticles and the surfactant, which is used based on the electric polarization of the surfactant to prevent agglomeration of the nanoparticles, together with tensional as well as gravitational forces in the ferrofluids make them extremely complex compounds. Superlattices and self-assembled iron-oxides nanocrystals have also many industrial applications especially in magnetic recording media and hence recently attracted considerable amount of attention [14–19].

Another interesting class of materials is ferrites. The parent

* Corresponding author.
E-mail address: skamali@utsi.edu (S. Kamali).
URL: http://www.utsi.edu (S. Kamali).

http://dx.doi.org/10.1016/j.jmmm.2015.12.007
0304-8853/

compound, i.e., magnetite (Fe_3O_4), is a ferrimagnetic compound with two different cation sites in a unit cell: 8 tetrahedral A sites, and 16 octahedral B sites. Magnetite is an inverse spinel, in other words, $(Fe^{+3})[Fe^{+2}Fe^{+3}]O_4$, where the parentheses stand for the tetrahedral sites and the square parentheses stand for the octahedral sites. Furthermore, the Fe^{+3} ion has a magnetic moment of 5 μ_B and the Fe^{+2} ion has 4 μ_B resulting in total magnetic moment of 4 μ_B. Above the Verwey [20] transition temperature there is a free electron hopping between Fe^{+2} and Fe^{+3} in the B sites, causing magnetite to be a conductor. Below the Verwey transition temperature this electron is frozen and the magnetite will be an insulator. Concerning the above-mentioned magnetic and electrical properties of magnetite, it is possible to introduce 3*d* transition metals in magnetite, hence manipulate and control these properties.

It is well-known that in contrast to metallic alloys where Ni and Co, in relatively low concentrations, increase the Fe magnetic moment according to the Slater–Pauling curve [21], the magnetization is decreased when such elements are incorporated into magnetite compared to the pure magnetite [22,23]. On the other hand, the Fe magnetic hyperfine field is increased both in metallic alloys [24–26] and in such ferrites [23,27].

Mössbauer spectroscopy has been proven to be a powerful technique for characterization of different iron-oxide nanoparticles [28–30], identifying their coexistence in a nanoparticle [31], or in solid solutions [32]. Furthermore, it is a suitable technique to gain insight into the distribution of cations in ferrites [23,27]. Accordingly, this technique is suitable for characterization of iron-oxide-based ferrofluids.

Furthermore, as orbital magnetic moment in most iron-oxides is quenched, the dominant magnetic moment in this class of magnetic material is the spin magnetic moment. Spin-polarized electron momentum densities (EMDs) can be studied by magnetic Compton scattering (MCS) [33]. It is called magnetic Compton profile (MCP) [34] of magnetic atoms:

$$J_{mag}(p_z) = \int_{-\infty}^{+\infty}\int_{-\infty}^{+\infty} n_{mag}(\mathbf{p})\, dp_x\, dp_y. \tag{1}$$

$\mathbf{p} = (p_x, p_y, p_z)$ is the electron momentum and $n_{mag}(\mathbf{p})$ is the spin-polarized EMD,

$$n_{mag}(\mathbf{p}) = n_{up}(\mathbf{p}) - n_{down}(\mathbf{p}), \tag{2}$$

where $n_{up}(\mathbf{p})$ and $n_{down}(\mathbf{p})$ are up-spin and down-spin EMDs respectively, defined as,

$$n_{up/down}(\mathbf{p}) = \sum_i \left| \int \psi_{i,up/down}(\mathbf{r}) \exp(-i\mathbf{p}\cdot\mathbf{r})\, d\mathbf{r} \right|^2, \tag{3}$$

as a function of the up-spin and down-spin electron wave functions $\psi_{i,up/down}(\mathbf{r})$. The summation in Eq. (3) extends over all occupied states. The p_z-axes is taken along the scattering vector. The shape of MCP depends on the spin-polarized atomic species, their local structures and the direction of scattering vector. In general, Compton scattering refers to x-ray scattering in a deeply inelastic regime, because x-rays interact not only with the electron charge but also with the electron spin. Therefore, MCP, which is the difference between the majority- and the minority-spin Compton profiles, can be extracted by measuring two Compton scattering cross-sections: one in the direction of magnetization of the specimen parallel to the scattering vector, and the other in the anti-parallel direction of magnetization. MCS has proved to be a powerful technique for characterization of different nanostructures [14,35–38].

This study has a two-fold motivation. The first is to investigate the stability of a Co-ferrite, $CoFe_2O_4$, ferrofluid after more than two decades of its preparation. The second is to characterize it with powerful techniques to gain insight into its magnetic properties as well as the electron polarization and atomic arrangement. The structure and morphology of the nanoparticles were investigated by transmission electron microscopy (TEM), high-resolution TEM (HR-TEM), and x-ray diffraction (XRD), while energy-dispersive x-ray spectroscopy (EDS) provides information about the elemental distribution.

2. Experimental details

The synthesis of the ferrofluid was based on the wet-grinding approach the details of which can be found elsewhere [39]. The compound was prepared more than two decades ago and has been kept in the ambient atmosphere. The structure of the nanoparticles in the ferrofluid was investigated by XRD using a Philips X'Pert diffractometer equipped with a copper tube in Bragg–Brentano geometry operating at 45 kV/40 mA, together with a Lynx-eye energy dispersive position sensitive detector (3° opening). The radiation used was CuK_α (λ = 1.5418 Å). The crystal structures were refined using the Rietveld method [40] implemented in the FullProf software [41]. Zero point and displacement error were refined using an internal Si standard (a=5.430922 Å, NIST 640b). The instrumental resolution was determined by measurements of a LaB_6-standard (NIST 660).

The morphology and dimensions of the synthesized nanoparticles in the ferrofluid were determined by HR-TEM using a Philips CM12 transmission electron microscope, and the average diameter of the Co-ferrite nanoparticles was determined by measuring the diameters of 200 particles and fitting the histograms to Gaussian distribution function. The EDS measurements were performed in conjunction with FEI XL30-SFEG scanning electron microscopy operating at a voltage of 10 kV.

A conventional transmission ^{57}Fe Mössbauer spectrometer, working in constant acceleration mode, was used for this experiment. The movement of the radioactive source, ^{57}Co in Rh matrix held at room temperature (RT), was controlled by a computerized interface. The sample was mounted in a He-flow cryostat and spectra were recorded at 10, 50, 80, and 300 K. The recorded spectra were analyzed using the software Recoil [42]. All centroid shifts, δ, are given with respect to metallic α-iron at RT.

The MCS experiment was carried out at the BL08W beamline of SPring-8. The incident x-rays, with 175 keV energy, were elliptically polarized and perpendicular to the sample surface. Energy spectra of Compton-scattered x-rays were measured at 10 K, in a magnetic field of +2.5 T (parallel to the scattering vector) and −2.5 T (anti-parallel to the scattering vector). The MCS contributions were separated by taking the difference between the energy spectra at +2.5 T and −2.5 T. The measurement was repeated using the sequence of magnetic fields, ABBABAAB, where A is +2.5 T and B is −2.5 T, with a data-accumulation duration of 60 s each. The energy spectra of the MCS x-rays were converted to MCP using a standard data-processing method [43].

3. Results and discussion

A typical XRD pattern for the sample is shown in Fig. 1. The XRD diffractogram has relatively sharp peaks, indicating an excellent crystallinity, as it is evident from (220), (311), (222), (400), (422), (511), and (440) peaks, which are typical for inverse spinel structure nanoparticles [44]. The broadening of the peaks is an indication of the finite size in accordance with the Scherrer equation [45]:

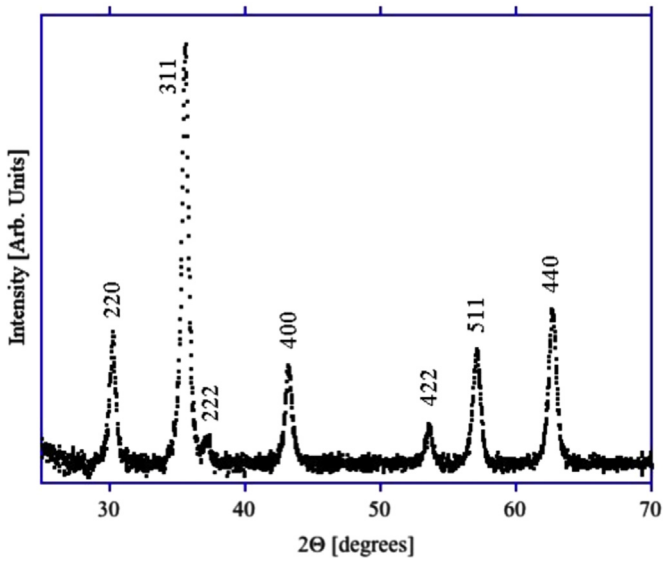

Fig. 1. The XRD pattern of the ferrofluid sample.

$$d = \frac{\beta\lambda}{B_{1/2}\cos(\theta)}. \quad (4)$$

where β is 0.94, wavelength λ of 1.5418 Å, B is the full width at half maximum (FWHM) of the peaks, and θ is the diffraction angle. FWHM of the instrument is below 0.12° for $20 \le 2\theta \le 120°$, and about one order of magnitude smaller than FWHM refined for the samples for $20 \le 2\theta \le 70°$, thus all peak-broadenings observed for the sample are from the sample and not from the diffractometer. Using (311) peak, which has the strongest diffraction, results in a size of 19.4 nm.

A TEM image of the sample is illustrated in Fig. 2. As seen in the HR-TEM indicated in the inset in Fig. 2, the crystal planes are clearly seen in the nanoparticles extending to the surface. The average particle diameter of $d = 18 \pm 1$ nm for the nanospheres is extracted from the TEM image. The content of the nanoparticles,

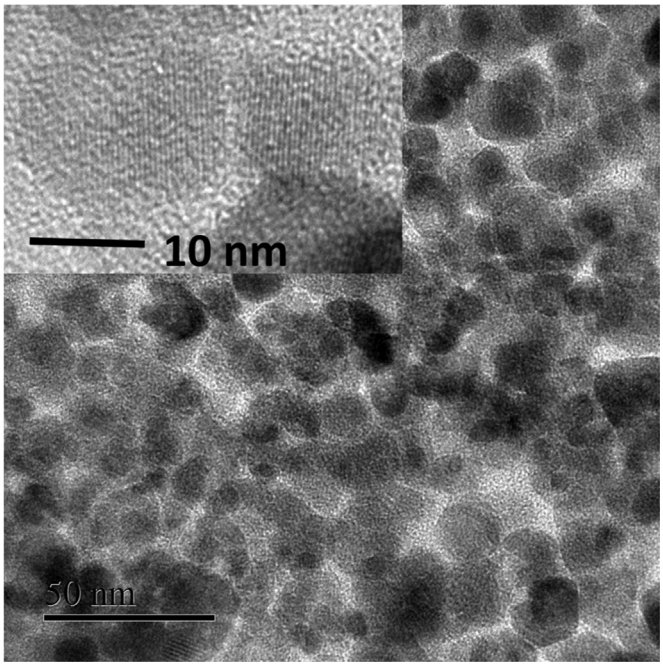

Fig. 2. A TEM micrograph of the ferrofluid sample. The inset is an HR-TEM graph showing the crystal planes extending to the surface.

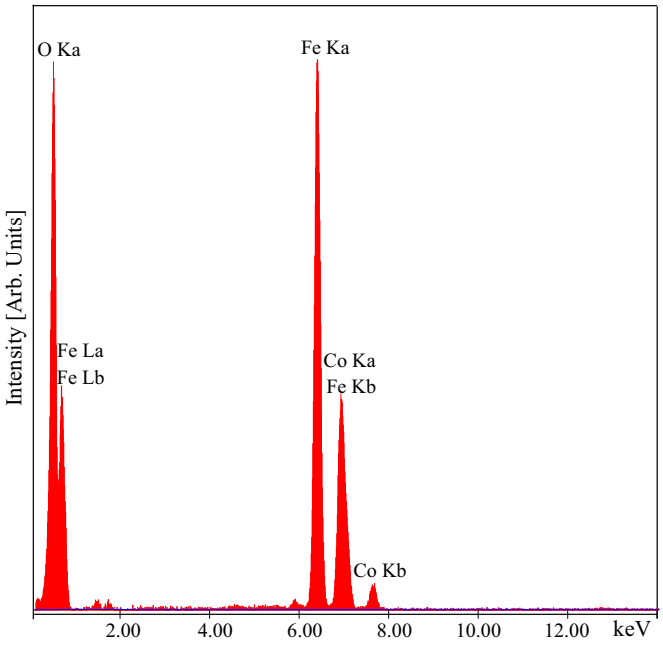

Fig. 3. EDS spectrum for the ferrofluid sample.

Fe, Co, and O, is seen in Fig. 3. The ratio of intensities is close to $CoFe_2O_4$.

The Mössbauer spectra measured from 150 K down to 10 K are shown in Fig. 4. Using three components results in the best fit of the Mössbauer spectra. The hyperfine parameters from the fit are summarized in Table 1. The first two components in 10 K spectrum have δ values of 0.461 mm/s and 0.510 mm/s, which are typical for Fe^{+3} in the octahedral sites. The high B_{hf} values are not only due to low temperature, but also due to Fe atoms having Co atoms as neighbors [25,23,27]. The intensities of these components are 28% and 41%. The third component has a δ value of 0.359 mm/s, which is typical for Fe^{+3} in tetrahedral site. The intensity of 31% for this component results in cation distribution of $(Co_{0.38}Fe_{0.62})[Co_{0.62}Fe_{1.38}]O_4$. As there is no Fe^{+2}, all Co atoms are in Co^{+2} to preserve charge neutrality of the compound.

Fig. 5 shows the MCP measured at 10 K.

The MCP is very similar to that of a spherical maghemite nanocrystalline sample [14]. It contains two components, namely, a broad positive 3d profile, and a narrow negative contribution which makes a dip at $p_z=0$. The dip is caused by the negative spin-polarization of the Fe atom at the tetrahedral A site [46], in which the Fe 3d states are strongly hybridized with the ligand O 2p states. In our previous study on maghemite nanocrystals [14], we used the full potential linearized augmented plane wave method within the local spin density approximation to calculate the theoretical MCPs of magnetite, which has similar structure to maghemite, along the [100], [110] and [111] directions as shown in Fig. 6.

It was shown that while theoretical MCPs along the [110] and [111] directions had clear peaks at $p_z=0$, the MCP along the [100] direction had a large peak around 1.1 atomic units (a.u.), and a dip at $p_z=0$. It is an interesting observation that despite the fact that inverse spinels have [111] as their easy axis, the nanoparticles in this ferrofluid align themselves along [100] direction, parallel to the external magnetic field, due to their freedom to rotate in an external magnetic field. The dip at low electron momentum regions is slightly deeper compared to typical MCPs in magnetite and maghemite [14,47], which is due to higher concentration of Co in B-sites. As Co atoms have lower spin moment compared to Fe atoms, the strength of the magnetic moment in the A-site is

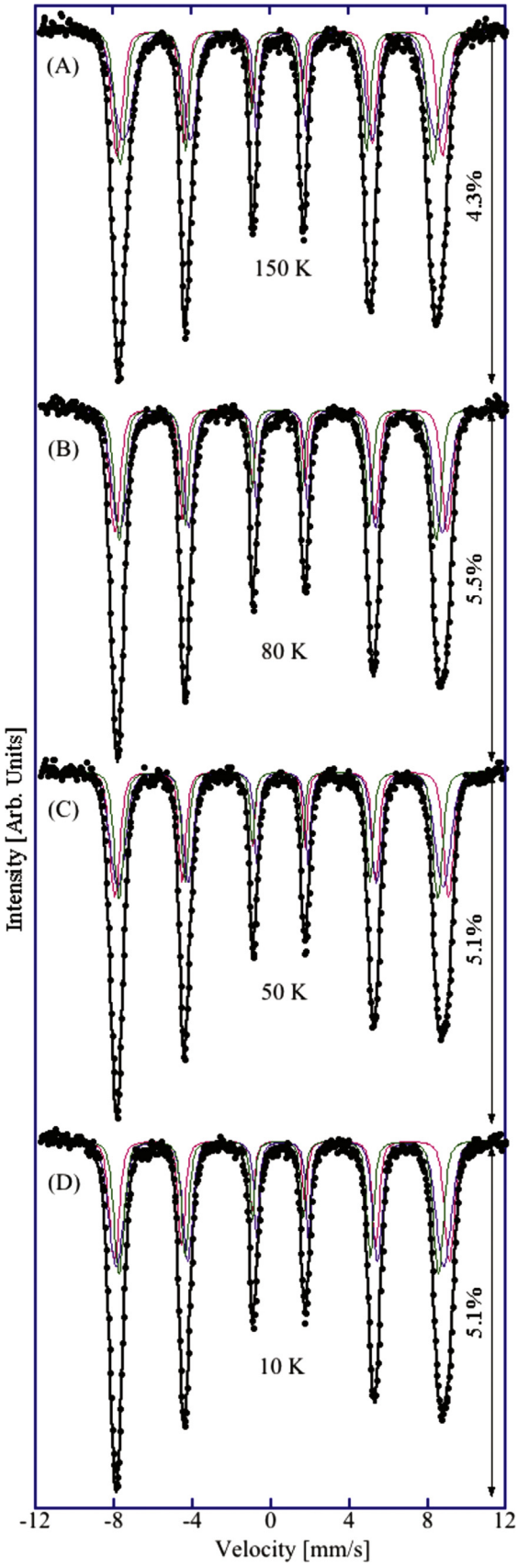

Fig. 4. Mössbauer spectra of the ferrofluid sample recorded at different temperatures.

Table 1
Mössbauer parameters of the sample measured at different temperatures: the magnetic hyperfine fields (B_{hf}), magnetic hyperfine field distributions (σ), centroid shift (δ), quadrupole shift (ϵ), and intensities (I) of the different components. Estimated errors in B_{hf} are $\pm$ 0.2 T, in σ, $\pm$ 0.2 T, in δ and ϵ, $\pm$ 0.01 mm/s, and in I, $\pm$ 3%.

Subspectra	10 K	50 K	80 K	180 K
$B_{hf,1}$ (T)	53.1	52.9	52.7	51.5
σ_1 (T)	1.2	1.3	1.3	1.4
δ_1 (mm/s)	0.461	0.464	0.448	0.423
ϵ_1 (mm/s)	0.079	0.070	0.058	0.042
I_1 (%)	28	30	29	29
$B_{hf,2}$ (T)	51.9	51.5	51.2	49.6
σ_2 (T)	2.0	2.1	2.1	2.8
δ_2 (mm/s)	0.510	0.517	0.524	0.511
ϵ_2 (mm/s)	−0.064	−0.054	−0.037	−0.026
I_2 (%)	41	40	41	41
$B_{hf,3}$ (T)	50.6	50.5	50.3	49.4
σ_3 (T)	1.2	1.1	1.2	1.4
δ_3 (mm/s)	0.359	0.343	0.326	0.300
ϵ_3 (mm/s)	0.024	0.020	0.014	0.012
I_3 (%)	31	30	30	30

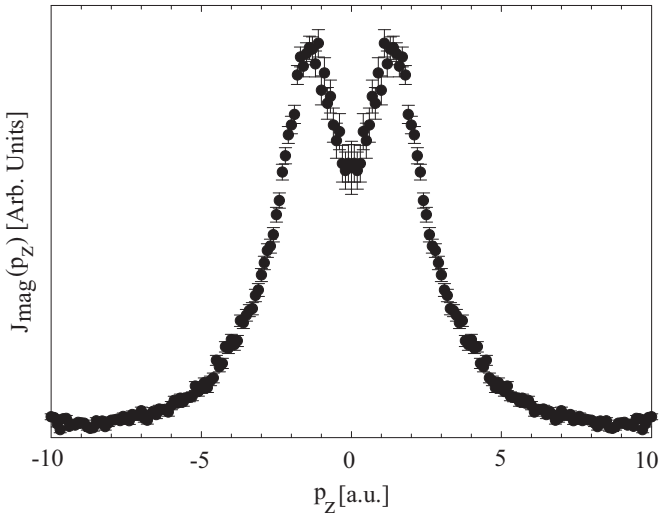

Fig. 5. MCP of the ferrofluid sample measured at 10 K.

increased relative to the magnetic moment in the B-sites according to the model presented in our previous work [46].

The stability of a ferrofluid is shown in its response to an external magnetic field. In case of magnetic nanoparticles suspended in a solution, only the nanoparticles are attracted to an external magnetic field. On the other hand, when a ferrofluid is exposed to an external magnetic field, the whole sample will be attracted to the external field, and spikes are formed, as shown in Fig. 7 for this ferrofluid. The response is identical to the ferrofluid's response to an external magnetic field when it was synthesized more than two decades ago (not shown). Besides the results from the characterization techniques used in this study, i.e., Mössbauer spectroscopy, which shows the existence of Co and Fe in the nanoferrite, and MCP showing the existence of a Co-based ferrite, the visible response of the ferrofluid to an external magnetic field shows that the ferrofluid is still stable after more than two decades.

4. Conclusions

In this work XRD, HR-TEM, EDS, Mössbauer spectroscopy, and MCS have been used to characterize the structural and magnetic

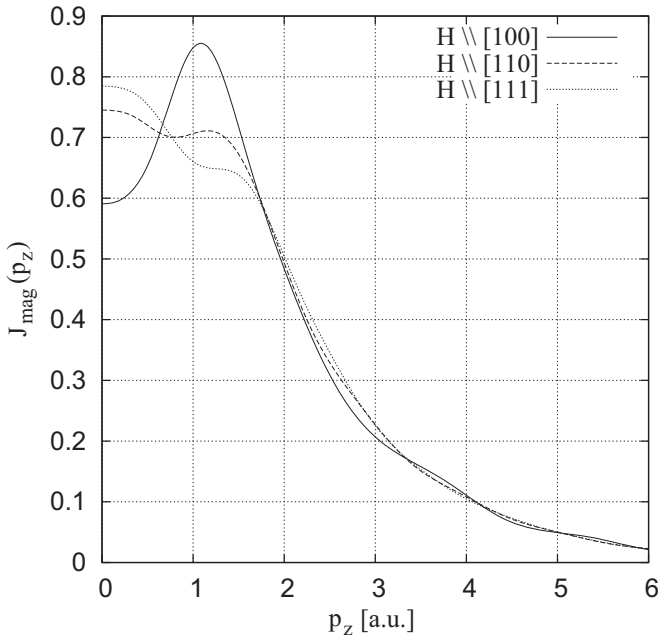

Fig. 6. Theoretical magnetic Compton profiles of Fe_3O_4 along the [100], [110], and [111] directions. Reprinted with permission from Kamali et al. [14]. © 2012 The American Physical Society.

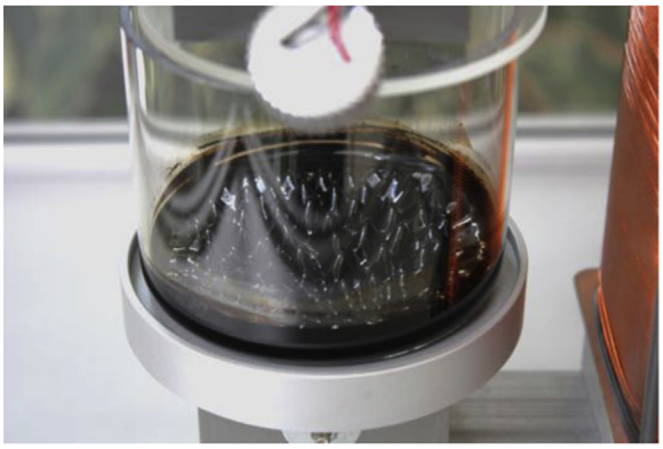

Fig. 7. Response of the ferrofluid to an external magnetic field.

properties of a cobalt-ferrite ferrofluid. It is demonstrated that this ferrofluid is still stable after more than two decades. Mössbauer spectroscopy gives the cation distribution, which is $(Co_{0.38}Fe_{0.62})[Co_{0.62}Fe_{1.38}]O_4$. Finally, the spin moment in these nanoparticles are aligned in [100] direction in external 2 T magnetic field, despite the fact that the easy axis in ferrites is [111] direction.

Acknowledgments

We would like to thank Henri Saljougui for technical assistance in preparing this paper. We appreciate Fred Hayes' assistance in TEM measurements. Saeed Kamali acknowledges Japan Society for the Promotion of Science for financial support. The magnetic Compton scattering experiment was performed with the approval of the Japan Synchrotron Radiation Research Institute (Proposal no. 2010B1294).

References

[1] J. Poppelwell, S. Charles, New Sci. 87 (1980) 332.
[2] R.E. Rosensweig, Sci. Am. 247 (1992) 136.
[3] J. Fidler, T. Schrefl, W. Scholz, D. Suess, V.D. Tsiantos, R. Dittrich, M. Kirschner, Physica B 343 (2004) 200.
[4] S. Sun, C.B. Murray, J. Appl. Phys. 85 (1999) 4325.
[5] B.A. Holm, E.J. Bergey, T. De, D.J. Rodman, R. Kapoor, L. Levy, C.S. Friend, P. N. Prasad, Mol. Cryst. Liq. Cryst. 374 (2002) 589.
[6] R. Hergt, W. Andrä, C.G. d'Ambly, I. Hilger, W.A. Kaiser, U. Richter, H. G. Schmidt, IEEE Trans. Magn. 34 (1998) 3745.
[7] J. Tucek, R. Zboril, D. Petridis, J. Nanosci. Nanotechnol. 6 (2006) 926.
[8] S. Kamali-M, T. Ericsson, R. Wäppling, Thin Solid Films 515 (1988) 721.
[9] L. Häggström, S. Kamali, T. Ericsson, P. Nordblad, A. Ahniyaz, L. Bergström, Hyperfine Interact. 183 (2008) 49.
[10] S. Mørup, J. Magn. Magn. Mater 37 (1983) 37.
[11] S. S. Papel, U.S. Patent 3 215 572.
[12] A. Dang, L. Ooi, J. Fales, P. Stroeve, Ind. Eng. Chem. Res. 39 (2000) 2269.
[13] B. Berkovski (Ed.), Magnetic Fluids and Applications Handbook, Begell House, New York, 1996.
[14] S. Kamali, M. Itou, A. Kodama, P. Stroeve, Y. Sakurai, Phys. Rev. B 85 (2012) 024506.
[15] S. Disch, E. Wetterskog, R.P. Hermann, G. Salazar-Alvarez, P. Busch, T. Brückel, L. Bergström, S. Kamali, Nano Lett. 11 (2011) 1651.
[16] C.J. Chen, R.K. Chiang, Y.-R. Jeng, J. Phys. Chem. C 115 (2011) 18142.
[17] S.C. Glotzer, M.J. Solomon, Nat. Mater. 6 (2007) 557.
[18] G.M. Whitesides, B. Grzybowski, Science 295 (2002) 2418.
[19] C.B. Murray, C.R. Kagan, M.G. Bawendi, Annu. Rev. Mater. Sci. 30 (2000) 545.
[20] E.J.W. Verwey, Nature (London) 144 (1939) 327.
[21] C. Kittel, Introduction to Solid State Physics, 7th edition, Wiley, New York, 1996.
[22] A.G. Bhosale, B.K. Chougule, Mater. Chem. Phys. 97 (2006) 273.
[23] F.L. Deepak, M. Bañobre-López, E. Carbó-Argibay, M.F. Cerqueira, Y. Pineiro-Redondo, J. Rivas, C.M. Thompson, S. Kamali, C. Rodríguez-Abreu, K. Kovnir, Y. V. Kolen'ko, J. Phys. Chem. C 119 (2015) 11947.
[24] S. Kamali-M, A.M. Blixt, L. Häggström, R. Wäppling, V. Stanciu, P. Nordblad, J. Magn. Magn. Mater. 1263 (2004) 272–276.
[25] S. Kamali-M, A. Bergman, G. Andersson, V. Stanciu, L. Häggström, J. Phys.: Condens. Mater 18 (2006) 5807.
[26] S. Kamali, L. Häggström, M. Sahlberg, R. Wäppling, J. Phys.: Condens. Mater 23 (2011) 055301.
[27] C.J. Chen, R.K. Chiang, S. Kamali, S.L. Wang, Nanoscale 7 (2015) 14332.
[28] A. Ahniyaz, G.A. Seisenbaeva, L. Häggström, S. Kamali, V.G. Kessler, P. Nordblad, C. Johansson, L. Bergström, J. Magn. Magn. Mater. 320 (2008) 781.
[29] S. Kamali, N. Shahmiri, J.S. Garitaonandia, J. Ångström, T. Ericsson, L. Häggström, Thin Solid Films 534 (2013) 260.
[30] N. Tarras-Wahlberg, S. Kamali, M. Andersson, C. Johansson, A. Rosén, J. Magn. Magn. Mater. 367 (2014) 40.
[31] Y. Kolen'ko, M. Bañobre-López, C. Rodriguez-Abreu, E. Carbó-Argibay, L. F. Deepak, D. Petrovykh, M.F. Cerqueira, S. Kamali, K. Kovnir, D.V. Shtansky, O. Lebedev, J. Rivas, J. Phys. Chem. 118 (2014) 28322.
[32] K.I. Lilova, F. Xu, K.M. Rosso, C.I. Pearce, S. Kamali, A. Navrotsky, Am. Mineral. 97 (2012) 164.
[33] N. Sakai, J. Appl. Cryst. 29 (1996) 81.
[34] N. Sakai, K. Ono, Phys. Rev. Lett. 37 (1976) 351.
[35] M. Ghafari, H. Hahn, H. Gleiter, Y. Sakurai, M. Itou, S. Kamali, Appl. Phys. Lett. 101 (2012) 243104.
[36] A. Stoesser, M. Ghafari, A. Kilmametov, H. Gleiter, Y. Sakurai, M. Itou, S. Kohara, H. Hahn, S. Kamali, J. Appl. Phys. 116 (2014) 134305.
[37] M. Ghafari, Y. Sakurai, G. Peng, Y.N. Fang, T. Feng, H. Hahn, H. Gleiter, M. Itou, S. Kamali, Appl. Phys. Lett. 107 (2015) 132406.
[38] S. Kamali, A. Kilmametov, M. Ghafari, M. Itou, H. Hahn, Y. Sakura, J. Phys.: Condens. Mater. 27 (2015) 075304.
[39] S. Odenbach (Ed.), Ferrofluids: Magnetically Controllable Fluids and Their Applications, Springer-Verlag, Berlin, Heidelberg, 2002.
[40] H.M. Rietveld, J. Appl. Crystallogr. 2 (1969) 65.
[41] J. Rodrguez-Carvajal, FullProf.2k Computer Program, Version 2.90 2.
[42] K. Lagarec, D. C. Rancourt, Recoil, Mössbauer Spectral Analysis Software for Windows, 1.0, Department of Physics, University of Ottawa, Canada, 1998.
[43] M.J. Cooper, et al. (Eds.), X-ray Compton Scattering, Oxford University Press, Oxford, 2004.
[44] H.M. Rietveld, S. Mahadevan, G. Gnanaprakash, J. Philip, T. Jayakumar, Physica E 39 (2007) 20.
[45] B.D. Cullity, S.R. Stock, Elements of X-ray Diffraction, 3rd edition, Prentice-Hall Inc., Massachusetts, 2001.
[46] S. Kamali, K. Shih, B. Barbiellini, Y.J. Wang, S. Kaprzyk, M. Itou, A. Bansil, Y. Sakurai, J. Phys: Condens. Mater. 27 (2015) 456003.
[47] H. Kobayashi, T. Nagao, M. Itou, S. Todo, B. Barbiellini, P.E. Mijnarends, A. Bansil, N. Sakai, Phys. Rev. B 80 (2009) 104423.